RECTANGULAR HOLLOW SECTION T-JOINTS UNDER DYNAMIC LOADS

L.M. El-Hifnawy, M.A.F. Diwan and M.M. EL-Heweity
Structural Engineering Department, Faculty of Engineering,
Alexandria University, Alexandria, Egypt.

ABSTRACT

The Unreinforced type of rectangular hollow sections T-joints is analyzed under dynamic loads. The chord top flange is modelled as a thin plate supported by coupled edge springs. The loadings are incorporated through line loads along the perimeter of a rigid inclusion (the branch member). The dynamic yield load is calculated and compared with the static yield load. From the results obtained, the Unreinforced joint is found to be very week under dynamic loads and the static yield load can be considered as a far conservative criterion for design purposes.

Keywords: Hollow sections, T-Joints, Dynamics.

INTRODUCTION

The joint in the Vierendeel girder may be subjected practically to dynamic loads resulting from earthquakes, machines, trains, etc. So far, there is no research done on hollow section considering dynamic loads. The R.H.S. T-joints model developed by Korol et al [4] is used to calculate the yield load carried by the joint under dynamic loads. The dynamic load used in the analysis is a simple harmonic sine load. Any general dynamic load (periodic) can be represented as the sum of a series of simple harmonic components by Fourier analysis. Therefore, knowledge of the harmonic case facilitates the treatment of more complicated types of excitation. The amplitude of the sine load is assumed to be the static yield load. Then the rigidity of the joint is examined for different frequencies of oscillation. The response is calculated in the time domain using the direct time integration method, *Wilson-θ* method. The well known program, SAP4, is used. A brief description of the multi-degree of freedom system, the direct time integration method and the generation of the load function is presented. The effects of the different parameters such as the frequency of oscillation, the damping ratio, ξ, and the number of model shapes on the dynamic yield load are studied. Then the results are compared with the static yield load obtained using the program developed by El-Hifnawy, L. [2] in order to evaluate the performance of the T-joints under dynamic load. The dynamic magnification factor, D, which is the ratio between the dynamic and static response of the joint is examined.

JOINT MODEL

The behavior of the single RHS joints (Figure 1) under punching shear is simulated by a two-dimensional model. The top flange of the chord member is treated as a thin plate supported by coupled springs along the edges Figure (2b). The remaining section resists the plate forces through frame action as indicated in Figure (3). Rollers are placed at points A and B to isolate localized joint behavior from chord member bending. A corner radius to the thickness ratio, r/t = 1, is assumed.

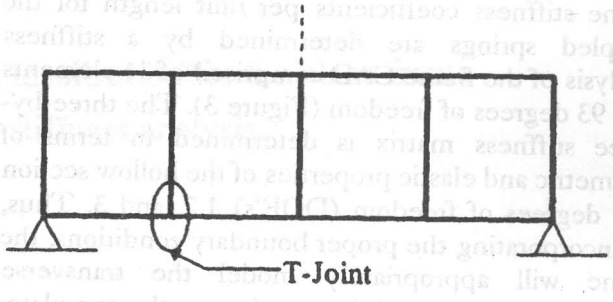

Figure 1. Vierendeel girder.

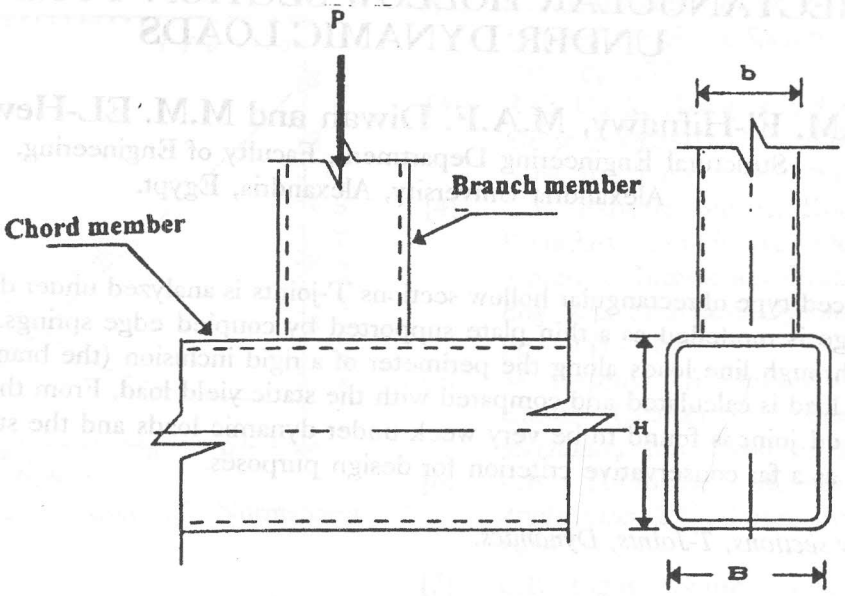

FIGURE 2. a ***Rectangular Hollow Section R.H.S. T-Joint.***

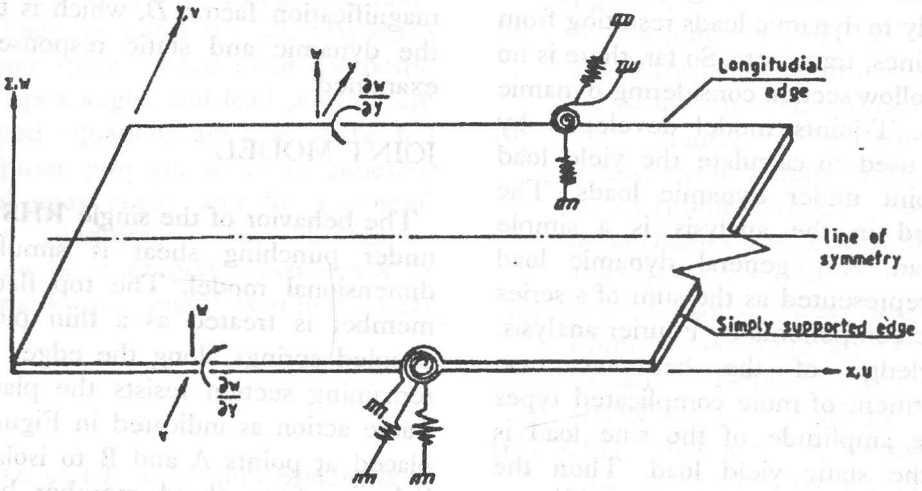

Figure 2b. Top flange of the chord member as a thin plate.

The stiffness coefficients per unit length for the coupled springs are determined by a stiffness analysis of the frame CAD comprised of 31 elements and 93 degrees of freedom (Figure 3). The three-by-three stiffness matrix is determined in terms of geometric and elastic properties of the hollow section and degrees of freedom (DOF's) 1,2, and 3. Thus, by incorporating the proper boundary conditions, the frame will appropriately model the transverse influence of the remaining section on the top plate. The spring coefficient matrix (3x3), for one-half of the chord, can then be obtained from the overall stiffness matrix for the frame by:

1. Setting the displacement at DOF number 73 (roller at A) and 91 (from symmetry), 93 (rotation at C), and 1 (neglecting in-plane action) to zero.
2. Setting DOF 1 equal to unity and DOF's 2 and 3 to zero,
3. Solving for the holding forces corresponding to DOF's 1,2, and 3. (These holding forces represent the first column in the required matrix of spring coefficients).

Step 2 and 3 are repeated for DOF's 3.

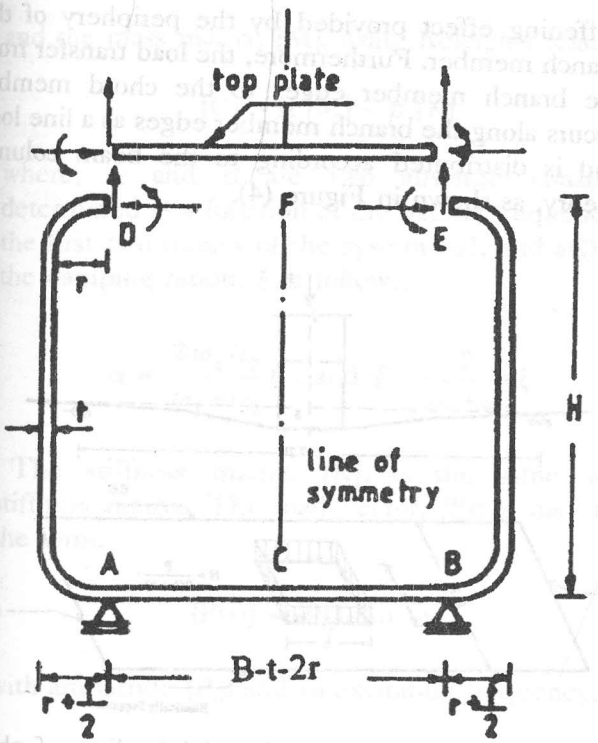

(a) Full Chord.

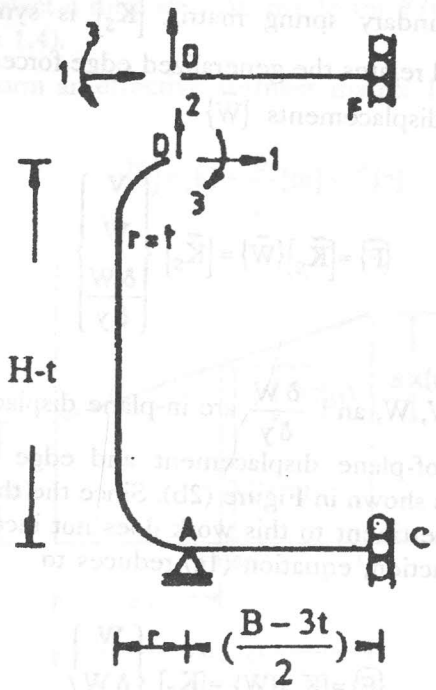

(b) One half the Chord.

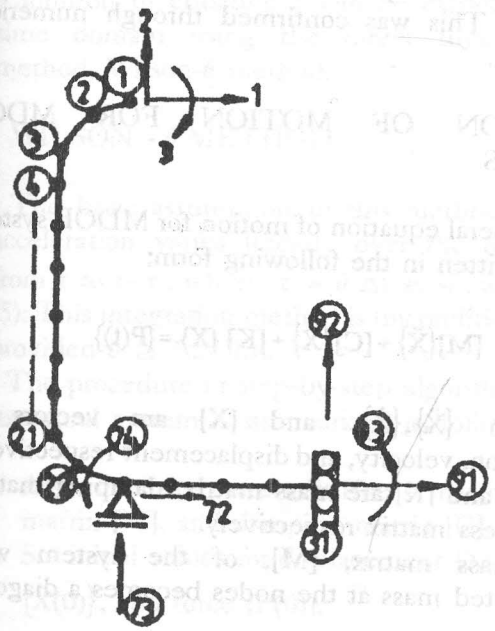

(c) Idealization for the plane frame stiffness analysis.

Figure 3. Modeling of the Chord member without the top flange.

The boundary spring matrix $[\bar{K}_S]$ is symmetric matrix and relates the generalized edge forces $\{\bar{F}\}$ to the edge displacements $\{\bar{W}\}$

$$\{\bar{F}\} = [\bar{K}_S]\{\bar{W}\} = [\bar{K}_S] \begin{Bmatrix} V \\ W \\ \frac{\delta W}{\delta y} \end{Bmatrix} \quad (1a)$$

Where V, W, and $\frac{\delta W}{\delta y}$ are in-plane displacement in y, out-of-plane displacement and edge rotation about x as shown in Figure (2b). Since the thin plate analysis pertinent to this work does not incorporate in-plane action, equation (1a) reduces to

$$\{\bar{F}\} = [K_S]\{W\} = [K_S] \begin{Bmatrix} W \\ \frac{\delta W}{\delta y} \end{Bmatrix} \quad (1b)$$

where $$[K_S] = \begin{bmatrix} K_v & K_{vr} \\ K_{rv} & K_r \end{bmatrix} \quad (2)$$

in which; K_v is the vertical spring constant, K_r the rotational spring constant, and $K_{vr} = K_{rv}$ is the coupling spring constant, respectively.

A typical elastic $[K_s]$ matrix for a 102 x 102 x 6.3 mm. chord with Young's modulus, E=2000 t/cm^2, and Poisson's ratio, $\upsilon = 0.3$ is

$$[K_s] = \begin{bmatrix} 109.25 & -809.75 \\ -809.75 & 380.65 \end{bmatrix} \quad (3)$$

(Units for K_v, K_r and K_{vr} are in KN/mm, KN/rad. and KN/rad., respectively.) Strong coupling existed among the spring constants indicating the inappropriateness of the simplified models with uncoupled flexibility coefficients as used by Redwood [8] and Korol and Mansour [5].

It is assumed that the branch member behaves as a beam column. The top flange plate of the chord member within the inclusion is assumed to undergo only rigid body type translation, δ, under concentrated force, P, This is so because of the stiffening effect provided by the periphery of the branch member. Furthermore, the load transfer from the branch member edges to the chord member occurs along the branch member edges as a line load and is distributed according to the beam column theory, as shown in Figure (4).

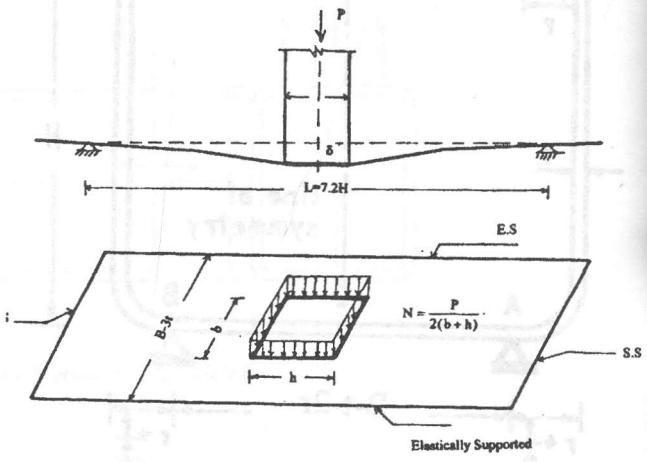

Figure 4. Model of branch axial loading of chord flange plate.

A chord flange plate length of 7.2 H has been used to model the joint behavior. This length was found to be sufficient to prevent any undesirable boundary restraints. This was confirmed through numerical testing [6].

EQUATION OF MOTION FOR MDOF SYSTEMS

The general equation of motion for MDOF system can be written in the following form;

$$[M]\{\ddot{X}\} + [C]\{\dot{X}\} + [K]\{X\} = \{P(t)\} \quad (4)$$

in which $\{\ddot{X}\}, \{\dot{X}\}$, and $\{X\}$ are vectors of acceleration, velocity, and displacement respectively, [M], [C], and [K] are mass matrix, damping matrix, and stiffness matrix respectively.

The mass matrix, [M], of the system with concentrated mass at the nodes becomes a diagonal matrix.

The damping matrix, [C], of the system may be taken as a combination of the stiffness matrix [K],

and the mass matrix, [M], using Releigh's relation,

$$[C] = \alpha [M] + \beta [K]$$

where, α and β are two absolute constants, determined as a function of the natural frequency of the first two modes of the system ($\omega 1$, and $\omega 2$) and the damping ration, ξ as follows,

$$\alpha = \frac{2\omega_1\omega_2}{\omega_1+\omega_2}\xi \text{ , and } \beta = \frac{2}{\omega_1+\omega_2}\xi$$

The stiffness matrix, [K], is the same static stiffness matrix. The load vector, {P(t)}, may take the form,

$$\{P(t)\} = \{P_o\} \text{ Sin } \bar{\omega} t$$

with amplitude $\{P_o\}$ and an excitation frequency, $\bar{\omega}$.

Then, the general equation of motion can be written as,

$$[M]\{\ddot{X}\} + [C]\{\dot{X}\} + [K]\{X\} = \{P_o\}\sin\bar{\omega} t \qquad (5)$$

Solution of equation 5 can be carried out in the time domain using the direct time integration method, Wilson-θ method.

WILSON - θ METHOD

The basic assumption of this method is that the acceleration varies linearly over the time interval from t to t+τ, where $\tau = \theta\,\Delta t$ as shown in Figure (5). This integration method is unconditionally stable provided $\theta \geq 1.37$ [3].

The procedure of step-by-step algorithm for linear structural system is summarized as follows [3]:

1. Assemble the system stiffness matrix [K], mass matrix [M], and damping matrix [C].
2. Set initial values for displacement {X(0)}, velocity $\{\dot{X}(0)\}$, and force {P(0)}.
3. Calculate initial acceleration $\{\ddot{X}(0)\}$ from,

$$[M]\{\ddot{X}(0)\} = \{P(0)\} - [C]\{\dot{X}(0)\} - [K]\{X(0)\}$$

4. Select a time step Δt, the factor θ (usually taken as 1.4).
5. Form an effective stiffness matrix $[\tilde{K}]$,

$$[\tilde{k}] = [k] + \frac{6}{\tau^2}[m] + \frac{3}{\tau}[c] \qquad (6)$$

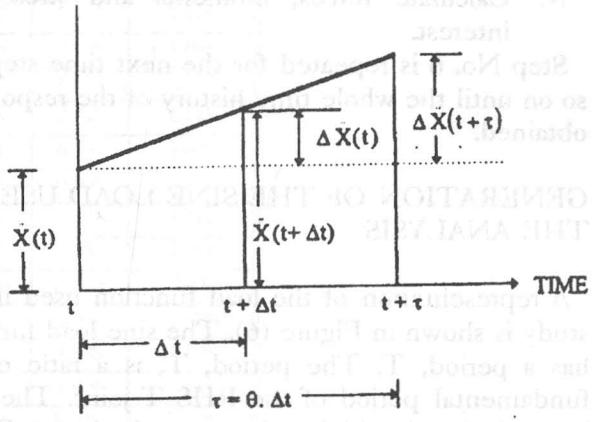

Figure 5. Linear acceleration assumption in the extended time interval.

6. For each time step:

i. Form an effective load vector $\{\Delta\tilde{P}\}$,

$$\{\Delta\tilde{P}\} = \{P(t)\} + \theta\{P(t+\Delta t) - P(t)\} + [m]\left(\frac{6}{\tau^2}\{X(t)\} + \frac{6}{\tau}\{\dot{X}(t)\} + 2\{\ddot{X}(t)\}\right)$$

$$+ [C]\left(\frac{3}{\tau}\{X(t)\} + 2\{\dot{X}(t)\} + \frac{\tau}{2}\{\ddot{X}(t)\}\right) \qquad (7)$$

ii. Solve for the effective displacement vector, $\{X(t+\tau)\}$ using the relation

$$[\tilde{K}]\{X(t+\tau)\} = \{\Delta\tilde{P}\} \qquad (8)$$

iii. Calculate new acceleration, velocity and displacement vectors,

$$\{\ddot{X}(t+\Delta t)\} = \left(1-\frac{3}{\theta}\right)\{\ddot{X}(t)\} + \frac{6}{\theta\tau^2}(\{X(t+\tau)\} - \{X(t)\}) - \frac{6}{\theta\tau}\{\dot{X}(t)\}$$

$$\{\dot{X}(t+\Delta t)\} = \{\dot{X}(t)\} + \frac{\Delta t}{2}(\{\ddot{X}(t)\} + \{\ddot{X}(t+\Delta t)\})$$

$$\{X(t+\Delta t)\} = \{X(t)\} + \Delta t\{\dot{X}(t)\} + \frac{\Delta t^2}{6}(\{\ddot{X}(t+\Delta t)\} + 2\{\ddot{X}(t)\}) \quad (9)$$

iv. Calculate forces, moments and stresses of interest.

Step No. 6 is repeated for the next time step and so on until the whole time history of the response is obtained.

GENERATION OF THE SINE LOAD USED IN THE ANALYSIS

A representation of the load function used in this study is shown in Figure (6). The sine load function has a period, T. The period, T, is a ratio of the fundamental period of the RHS T-joint. The time interval, Δt, should be chosen such that $\Delta t/T_n \leq 0.1$, where T_n is the period of the highest frequency to be taken into consideration. The amplitude of the sine load, P_o, is constant and is equal to the yield static load in order to compare between the response of the joint under the same value of static and dynamic loads. The frequency ratio, r, percentage of the fundamental frequency varies from 0.25 to 10.0 to study its effect on the joint yield dynamic load, P_{dy}.

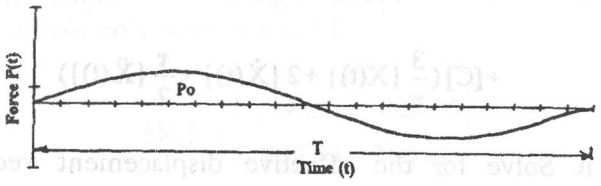

Figure 6. Representation of the sine load function used.

APPLICATIONS

A typical RHS T-joint is analyzed. The T-joint is of chord member size 102x102x6.3 mms, the top flange plate dimensions become 7.2H = 734.4 mm long and H-t-2r=83.1 mm. wide, and of branch member size 51x51x4.9 mms. A finite element mesh of 80 elements is considered. The density of the material used, steel= 7.8 t/m3, the Young's modules, E, =2000 t/cm2, and the yield stress, $\bar{\sigma}_o$ = 350 Mpa.

The R.H.S T-joint system is first solved as an eigen value problem in order to get the natural frequencies, ω, and the period, T, for each vibration mode. Table (1) shows these values for the first ten modes.

Table 1. Values for the first ten modes of the system in the joint used.

Mode shape no.	Natural frequency (ω) in rad/sec	Period (T) in sec.
1	29.69	0.21160
2	98.60	0.06372
3	104.70	0.06001
4	115.60	0.05433
5	132.00	0.04759
6	153.90	0.04082
7	181.00	0.03472
8	212.50	0.02957
9	247.20	0.02541
10	283.60	0.02216

For the joint analyzed, the program SAP4 is used to predict the yield dynamic load, P_{yd}, the corresponding maximum dynamic deflection, and moments. Also, the dynamic magnification factor of the joint, D, which is the ratio between the dynamic and the static responses, is calculated. The effect of number of modes, frequency ratio, r, and damping ratio, ξ, on the joint dynamic response is summarized in Tables (2) and (3) and Figures (7) to (14).

Table (2) and Figure (7) show the effect of the number of modes considered in the analysis on the dynamic magnification factor, D. It is clear that using lower modes (before 10 modes) of vibration only underestimates the response for low frequency ratios. Consequently, after 10 modes the response set to be approximately constant. For the range of frequency ratio (r<2) the dynamic response is 8 to 12 times the static response. On the other hand, for high frequency ratio (r>2), the response is not sensitive to the number of modes considered in the analysis. Also, Table (2) indicates that the increase of the damping ratio has the effect of decreasing the response.

Table 2. The dynamic magnification factor, D, of the Joint for different number of modes, frequency ratio, r, and damping ration, ξ.

No. of modes used	Frequency ratio (r)	Dynamic magnification factor (D)		
		ξ=0.5%	ξ=1.0%	ξ=5.0%
1	r=0.25	1.416	1.326	1.221
	r=0.50	2.028	1.957	1.824
	r=0.75	4.332	4.103	3.995
	r=0.80	5.857	5.499	5.014
	r=0.90	7.226	7.105	5.898
	r=1.00	8.702	8.378	6.300
	r=1.50	2.356	2.232	2.113
	r=2.00	1.046	0.996	0.886
	r=3.00	0.573	0.566	0.512
	r=4.00	0.430	0.424	0.411
	r=10.00	0.105	0.103	0.098
10	r=0.25	1.7018	1.6818	1.6234
	r=0.50	2.358	2.302	2.186
	r=0.75	5.006	4.898	4.156
	r=0.80	6.184	7.994	4.848
	r=0.90	10.334	10.886	7.170
	r=1.00	12.196	11.656	8.322
	r=1.50	2.670	2.610	2.284
	r=2.00	1.208	1.171	1.110
	r=3.00	0.684	0.680	0.649
	r=4.00	0.434	0.432	0.415
	r=10.00	0.134	0.133	0.128

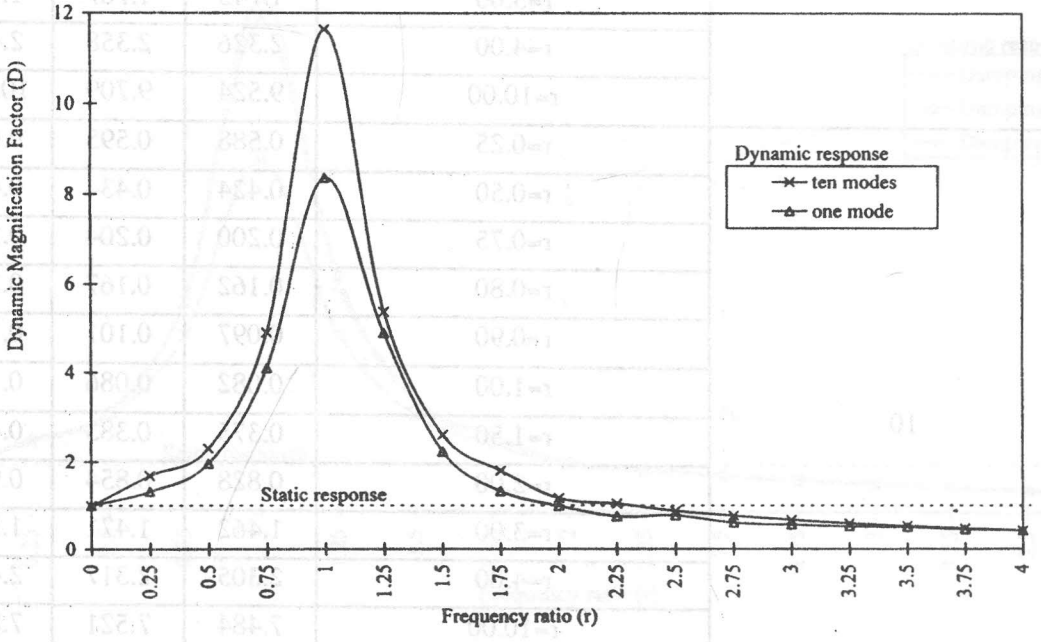

Figure 7. Effect of number of modes on the dynamics magnification factor for various frequency ratio using damping ratio =1.0%

Table (3) and Figures (8), (9) and (10) show how the ratio between the dynamic and static yield load is affected by the number of modes considered, the damping ratio, and the frequency ratio. It can be seen that the damping ratio has a minor effect on the dynamic yield load. For lower frequency ratios (r< 2), the dynamic yield load is less than the static yield load. For frequency ratio r=10, the dynamic yield load could be as much as 7 times the static yield load. Figures (11) to (14) show that the increase of the damping ratio has the effect of decreasing the maximum flange deflection and bending moments, as expected.

Table 3. The ratio between the dynamic yield load, P_{yd}, and the static yield load, P_{ys}, of the Joint for different number of modes, frequency ratio, r, and damping ratio, ξ.

No. of modes used	Frequency ratio (r)	Dynamic yield load (Pyd) / Static yield load (Pys)		
		ξ=0.5%	ξ=1.0%	ξ=5.0%
1	r=0.25	0.706	0.754	0.819
	r=0.50	0.493	0.511	0.548
	r=0.75	0.231	0.244	0.250
	r=0.80	0.171	0.182	0.199
	r=0.90	0.138	0.141	0.169
	r=1.00	0.115	0.119	0.159
	r=1.50	0.424	0.448	0.473
	r=2.00	0.956	1.004	1.129
	r=3.00	1.745	1.767	1.953
	r=4.00	2.326	2.358	2.433
	r=10.00	9.524	9.709	10.204
10	r=0.25	0.588	0.595	0.616
	r=0.50	0.424	0.434	0.458
	r=0.75	0.200	0.204	0.241
	r=0.80	0.162	0.167	0.206
	r=0.90	0.097	0.101	0.140
	r=1.00	0.082	0.086	0.120
	r=1.50	0.375	0.383	0.438
	r=2.00	0.828	0.854	0.901
	r=3.00	1.462	1.471	1.541
	r=4.00	2.305	2.317	2.411
	r=10.00	7.484	7.521	7.827

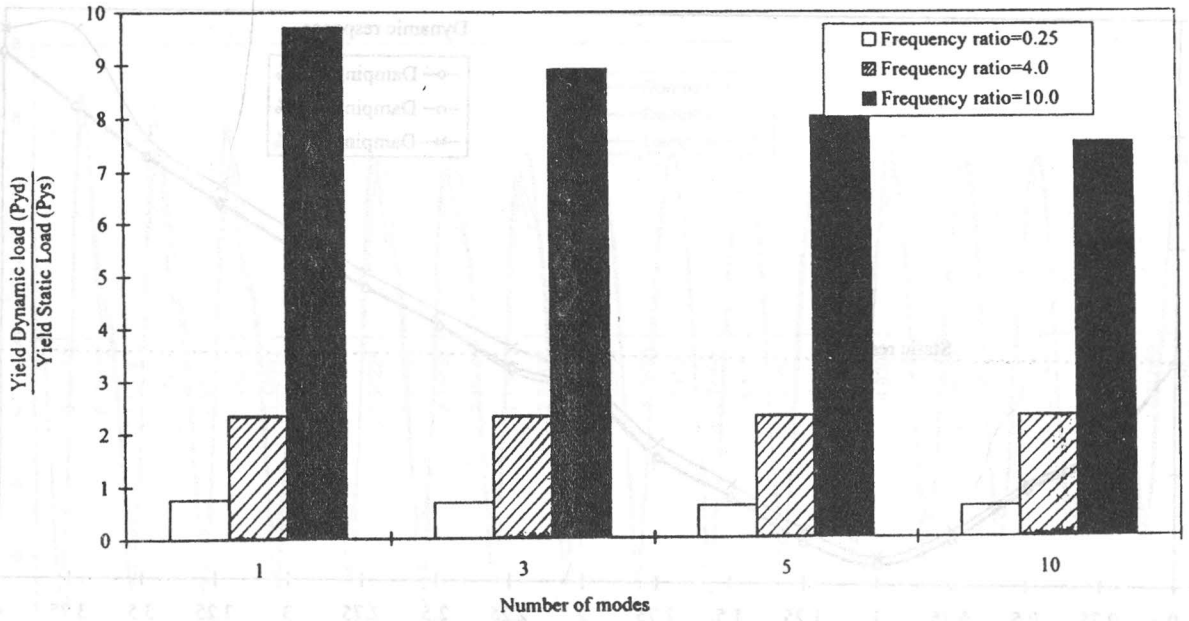

Figure 8. Effect of frequency ratio and number of modes on the ratio between the yield dynamic load and the yield static load.

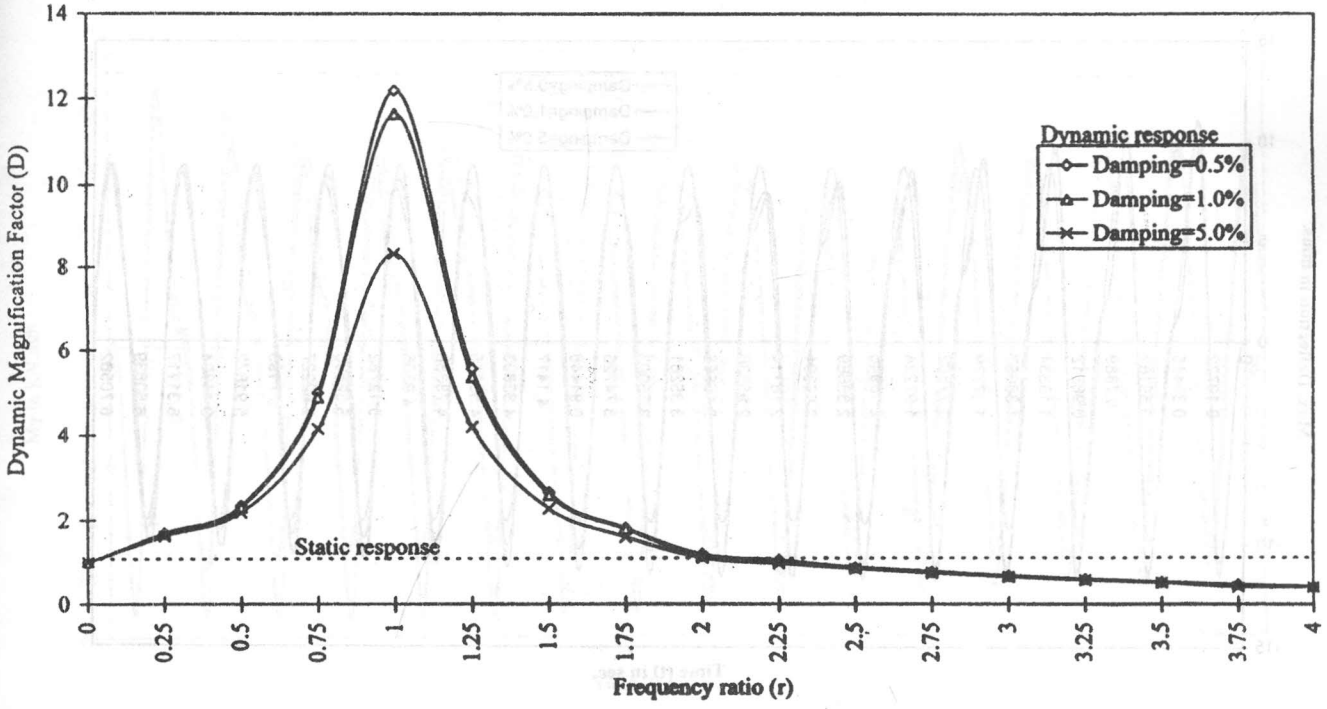

FIGURE 9 Effect of damping ratio on the dynamic magnification factor for various frequency ratio using ten modes.

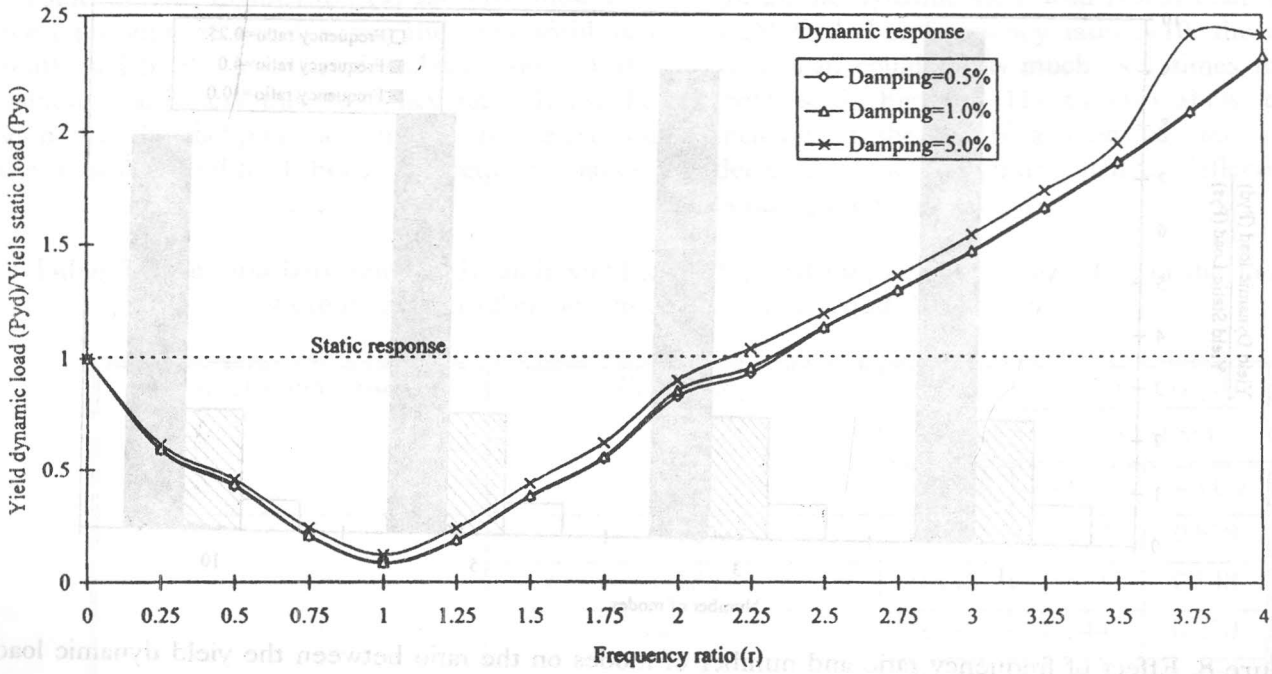

Figure 10. Effect of damping ratio on the ratio between the yield dynamic load and the yield static load for various frequency ratio using ten modes.

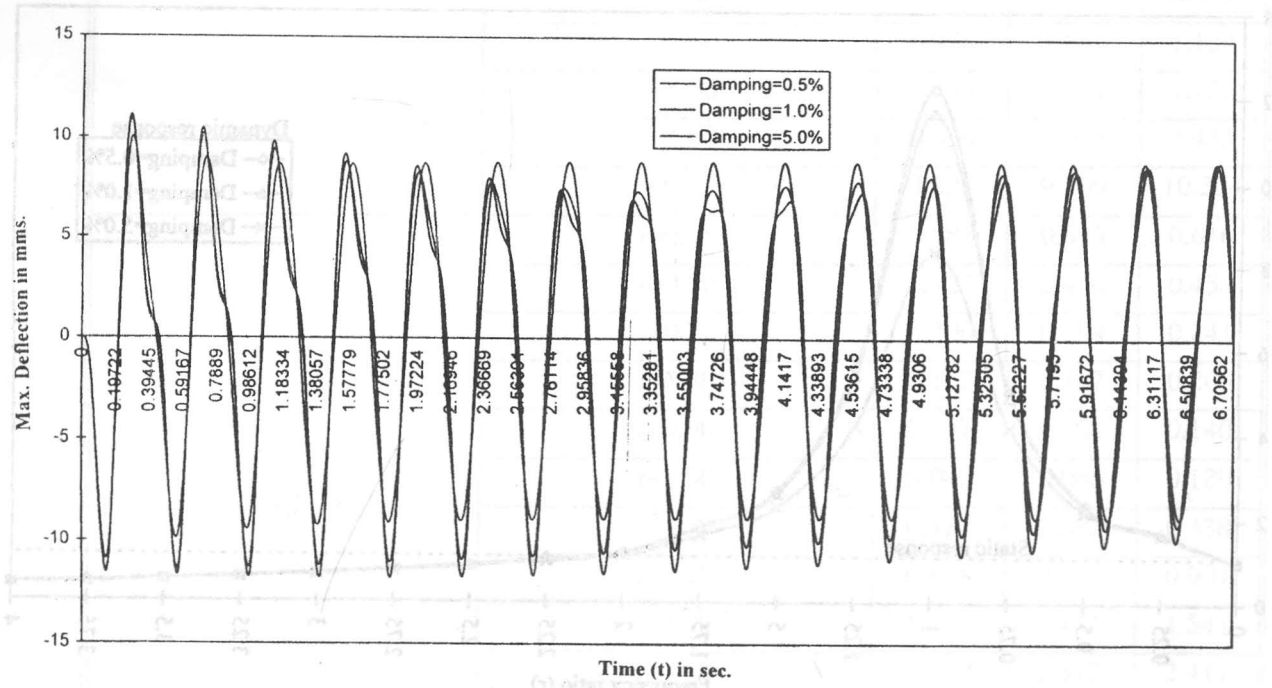

Figure 11. Effect of damping ratio on the history of the maximum deflection of the plate under dynamic load.

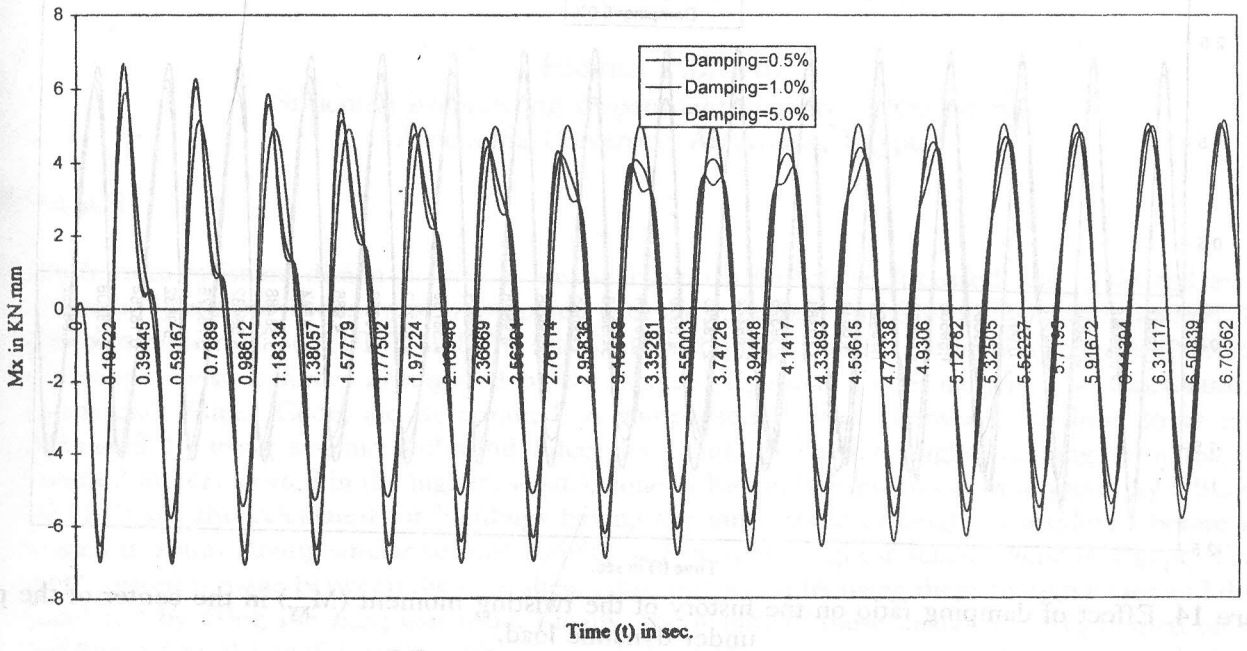

Figure 12. Effect of damping ratio on the history of the moment about x-axis (M_x) in the center of the plate under dynamic load.

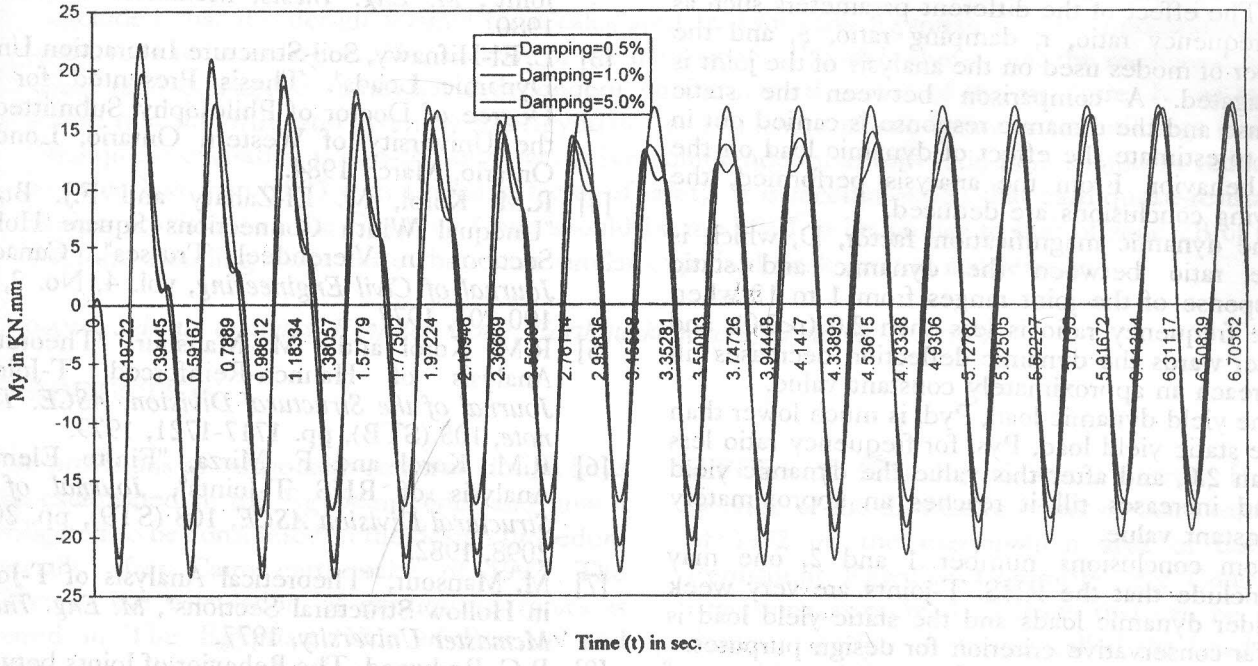

Figure 13. Effect of damping ratio on the history of the moment about y-axis (M_y) in the center of the plate under dynamic load.

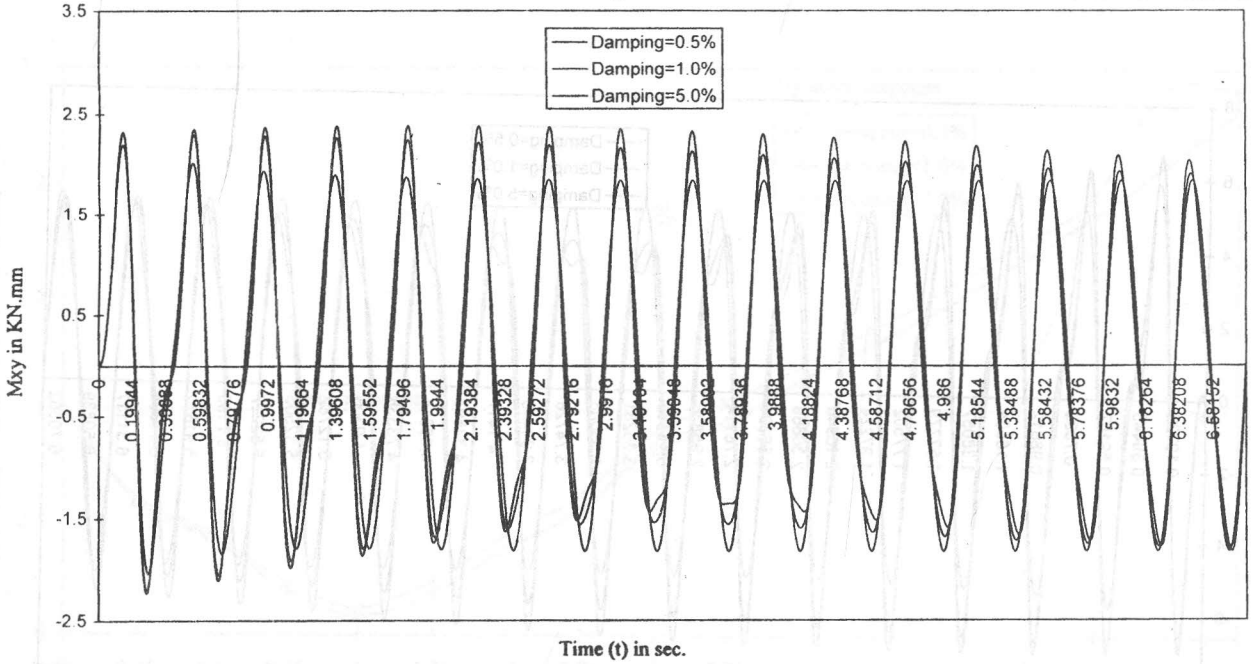

Figure 14. Effect of damping ratio on the history of the twisting moment (M_{xy}) in the center of the plate under dynamic load.

CONCLUSIONS

The behavior of the RHS T-joints under dynamic loading through the branch member in the elastic region is studied. The dynamic load is a harmonic sine load with amplitude equal to the yield static load. The effect of the different parameters such as the frequency ratio, r, damping ratio, ξ, and the number of modes used on the analysis of the joint is investigated. A comparison between the static response and the dynamic response is carried out in order to estimate the effect of dynamic load on the joint behavior. From the analysis performed, the following conclusions are deduced.

1. The dynamic magnification factor, D, which is the ratio between the dynamic and static response of the joint ranges from 1 to 12 when the frequency ratio is less than 2.0 (r<2.0), and after wards the dynamic deflection decreases till it reach an approximately constant value.
2. The yield dynamic load, Pyd, is much lower than the static yield load, Pys, for frequency ratio less than 2.0, and after this value the dynamic yield load increases till it reaches an approximately constant value.
3. From conclusions number 1 and 2, one may conclude that the RHS. T-joints are very week under dynamic loads and the static yield load is a far conservative criterion for design purposes.
4. The effect of damping ratio, x, on the response of the R.H.S T-joints is not significant as expected for steel structures.

REFERENCES

[1] M. Baz, *Structural Dynamic, Theory and Computation*, Chapman and Hall, 1991.

[2] L. El-Hifnawy, "Elasto-Plastic Finite Element Analysis of Rectangular Hollow Section T-Joint", *M. Eng. Thesis*, Mcmaster University, 1980.

[3] L. El-Hifnawy, Soil-Structure Interaction Under Dynamic Loads". Thesis Presented for the Degree of Doctor of Philosophy Submitted to the University of Western Ontario, London, Ontario, March 1984.

[4] R.M. Korol, M. El-Zanaty and F.J. Brady, "Unequal Width Connections Square Hollow Sections in Vierendeel Trusses", Canadian *Journal of Civil Engineering*, vol. 4, No. 2, pp. 190-201, 1977.

[5] R.M. Korol and M. Mansour, "Theoretical Analysis of Haunch-Reinforced T-Joints", *Journal of the Structural Division, ASCE. Tech. note*, 105 (STB), pp. 1717-1721, 1979.

[6] R.M. Korol and F. Mirza, "Finite Element Analysis of RHS T-Joints", *Journal of the Structural Division ASCE*, 108 (ST9), pp. 2081-2098, 1982.

[7] M. Mansour, "Theoretical Analysis of T-Joints in Hollow Structural Sections", *M. Eng. Thesis, Mcmaster University*, 1977.

[8] R.G. Redwood, The Behavior of Joints between Rectangular Hollow Structural Members", *Civil Engineering and Public Works Review*, vol. 6, No. 711, pp. 1463-1469, 1965.